Alignment relaxation of $Ne^*(2p_i[J=1])$ atoms induced by collisions with $He(1s^2)$ atoms in discharges at temperatures from 10 to 3000 K

Cristian Bahrim[1,*] and Vaibhav V. Khadilkar[1,2]

[1]*Department of Chemistry and Physics, Lamar University, Beaumont, Texas 77710-10046, USA*

[2]*Department of Computer Science, Erik Jonsson School of Engineering and Computer Science, The University of Texas at Dallas, Richardson, Texas 75080, USA*

(Received 21 December 2008; revised manuscript received 17 February 2009; published 29 April 2009)

Comparison between our close-coupling many-channel quantum calculations based on a model potential for the description of the interaction between atoms and accurate experiments of disalignment and destruction of alignment of the $Ne^*(2p_i[J=1])$ atoms induced by collisions with $He(1s^2)$ atoms in a gaseous mixture at thermal equilibrium is reported for temperatures between 10 and 3000 K. Our analysis leads to the conclusion that a good agreement with the various experiments is achieved when the dipole polarizability of the $Ne^*(2p_i[J=1])$ states is added to the long-range potentials proposed in Phys. Rev. A **56**, 1305 (1997) by Bahrim *et al.* Dipole polarizabilities for all the $Ne^*(2p_i[J=1])$ states of the $2p^5 3p$ electronic configuration are calculated.

DOI: 10.1103/PhysRevA.79.042715 PACS number(s): 34.10.+x, 34.20.−b, 34.50.−s

I. INTRODUCTION

Disalignment and destruction of alignment are two alignment relaxation processes for an axially symmetric ensemble of atoms. These processes offer accurate information about the anisotropic interaction between atoms in collision. An axially symmetric ensemble of atoms is aligned on the $|JM\rangle$ Zeeman states when the total electronic angular momentum $\vec{\mathbf{J}}$ is invariant under the reversal of the quantization z axis and the average projection $\langle \mathbf{J_z} \rangle$ is zero. In this case, the $|JM\rangle$ and $|J-M\rangle$ states are equally populated [1]. The disalignment of an ensemble of atoms is described by the temporal evolution of the electric quadrupole vector $\langle 3\mathbf{J_z^2}-\vec{\mathbf{J}}^2\rangle$, and in the density matrix formalism is represented by the evolution of the ρ_0^2/ρ_0^0 term, where ρ_0^2 and ρ_0^0 are the irreducible tensor components of rank 2 and 0, respectively [2]. The atomic disalignment is due to intramultiplet transitions between $|JM\rangle$ Zeeman states of the same fine-structure J state, while the destruction of alignment is due to both intra- and intermultiplet transitions between different J states [3].

In experiments of atomic disalignment induced by atomic collisions in a gaseous cell, the observable is the disalignment rate coefficient, which represents an energy-averaged cross section over the distribution of atoms in the cell. We will compare our disalignment rate coefficients based on quantum close-coupling many-channel calculations with accurate experimental data [4–6] obtained through the analysis of polarized fluorescence from certain $J=1$ states of the $2p^5 3p$ configuration to the $1s_j$ states (where $j=2$, 3, and 4) using a laser-induced fluorescence spectroscopy (LIFS) technique. Based on measurements of Hanle signal emitted by polarized atoms [7], Carrington and Corney [8] have investigated the destruction of alignment. To the best of our knowledge, their old measurements still offer the most accurate data available in literature for the destruction of alignment of the $Ne^*(2p_i)$ atoms (where $i=2,\ldots,10$) induced by collisions with $He(1s^2)$ atoms. Fujimoto and Matsumoto [3] have shown that the destruction of alignment measured in [7,8] is different than the disalignment of atoms measured using the LIFS method and concluded that the experimental technique used in Refs. [7,8] should necessarily include the information about both intermultiplet and intramultiplet transitions. The depopulation of the $2p_i$ level due to intermultiplet transitions represents the sum of the excitation transfer toward other $2p_k$ ($k=1$ to 10 and $k\neq i$) levels [9]. The interpretation proposed in [3] for experiments done in [7,8] was validated later by elaborate quantum calculations performed by Bahrim *et al.* [10].

In this paper we will compare our quantum close-coupling many-channel calculations based on potential energies from Refs. [11,12] with accurate experimental data for alignment relaxation (disalignment [4–6] and alignment destruction [8]) of $Ne^*(2p_i[J=1])$ atoms induced by Ne^*-He collisions. The potential energies from [11] have improved the potentials constructed by Hennecart and Masnou-Seeuws in [13] (who have proposed an excellent model potential for the interaction between the low-lying Ne^* atoms and the He ground-state atoms) with the inclusion of accurate core-core potentials for the He $Ne^+(2p^5)$ molecular ion and new long-range potentials for the $e^-(3p)-$He interaction at internuclear distances from 15 to 20 a_0.

The present analysis will lead us to the hypothesis that an accurate description of the alignment relaxation of $Ne^*(2p_i[J=1])$ atoms requires the addition of a state-dependent dipole polarization potential to the long-range potentials from [11]. This hypothesis will be tested for the alignment relaxation of $Ne^*(2p_i[J=1])$ atoms induced by Ne^*-He collisions in a gaseous mixture at thermal equilibrium for a wide temperature range, from 10 to 3000 K and comparison with measurements from Refs. [4–6,8] will be reported.

Studies of the atomic alignment relaxation are important in any quantitative analysis of the plasmas using a collisional-radiative model [14]. In general, the analysis of

*Corresponding author; cbahrim@my.lamar.edu

the polarization characteristics of the radiation emitted by atoms in plasmas gives essential information about how these atoms were excited [15]. Plasma polarization spectroscopy (PPS) is a sophisticated experimental technique which allows performing spectro-polarimetric observations of laboratory and celestial plasmas [14,15]. Both sets of experiments [4–6,8] that we use for comparison with our calculations apply a PPS technique for measuring the alignment relaxation of Ne^* atoms.

This paper is structured as follows: Sec. II gives a brief presentation of our quantum model. Section III presents a comparison between our quantum calculations for alignment relaxation of the $Ne^*(2p_i[J=1])$ atoms using our potentials from Refs. [11,12] and experimental data [4–6,8]. In Sec. IV we propose to modify the long-range potential for the $Ne^*(2p^5 3p)-He$ system from [11] by including the dipole polarizability of the $Ne^*(2p_2)$ atom. In Sec. V, we extend this model potential to the $2p_5$ and $2p_7$ levels introducing a state-dependent dipole polarization potential for the $Ne^*(2p_i[J=1])$ atoms (where $i=5$ and 7) to the long-range potentials from [11]. In this way an excellent agreement with the available experiments is found. In order to complete the set of theoretical data for all the $J=1$ states of the $2p^5 3p$ configuration of neon, in Sec. VI we calculate the alignment relaxation rates for the $Ne^*(2p_{10})$ atoms. Our conclusions follow in Sec. VII.

II. THEORETICAL MODEL

Details about the model potential for the Ne^*-He system and the close-coupling many-channel method adopted in our quantum calculations were already presented in Ref. [11]. The basic formulas for our calculations of alignment relaxation cross sections and rate coefficients were reported in Refs. [10,12]. The alignment destruction rate of the $Ne^*(2p_i[J=1])$ atoms is defined as the ratio between the sum of the rate coefficients for disalignment between the $M=0$ and 1 Zeeman states and the total de-excitations from that $2p_i$ state toward other $2p_k$ states (where $i \neq k$), and the average velocity, $\bar{v}$, of the reduced mass particle, μ, of the He Ne^* system (of 3.34 amu)

$$\sigma^{(2)} = \frac{\left[K^{DA} + \sum_{i \neq k} K_{2p_i \to 2p_k}\right]}{\bar{v}}, \tag{1}$$

$$\text{where } K^{DA} = \int_0^\infty 3\sigma_{01}(E)\sqrt{\frac{2E}{\mu}} f(E) dE, \text{ and} \tag{2}$$

$$K_{2p_i \to 2p_k} = \int_0^\infty \sigma_{2p_i \to 2p_k}(E)\sqrt{\frac{2E}{\mu}} f(E) dE. \tag{3}$$

In Eqs. (2) and (3), $f(E)$ represents the Maxwell-Boltzmann energy distribution of atoms in the Ne^*-He gaseous mixture at temperature T. Both $\sigma^{(2)}$ and the rate coefficients defined in Eqs. (2) and (3) are calculated up to a temperature of 3000 K and for a range of collision energies, E, from 0.1 meV to 3 eV. Tests of convergence for our quantum calculations were carefully done and will be reported in this paper.

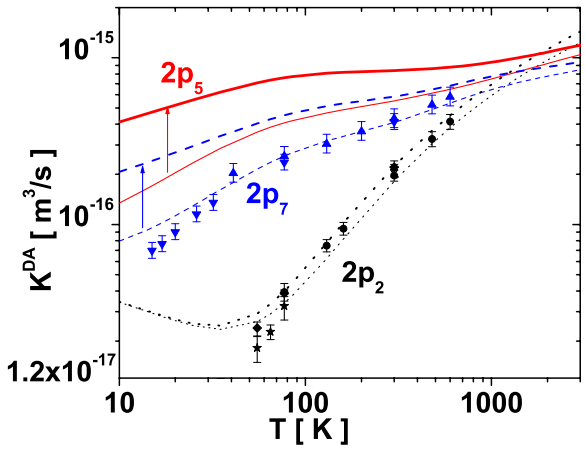

FIG. 1. (Color online) Disalignment rate coefficient (K^{DA}) of the $Ne^*(2p_2)$, $Ne^*(2p_5)$, and $Ne^*(2p_7)$ atoms: comparison between our quantum calculations for $2p_2$ (dotted lines), $2p_5$ (solid line), and $2p_7$ (dashed line) using the potentials from Refs. [11] (thin lines) and [12] (thick lines), and the experimental data for $2p_2$ from [4] (dots), [5] (diamonds), and [6] (stars), and for $2p_7$ from [4] (triangle up) and [5] (triangle down). The error bar is explicitly indicated. The arrows are used to indicate the shift upward of K^{DA} when potentials from Ref. [12] are used instead of those from Ref. [11].

Throughout our calculations, the effective time of collision τ_{col} is much larger than the characteristic time of the spin-orbit interaction τ_{so} for the $2p_i(J)$ states of the $Ne^*(2p^5 3p)$ configuration. We estimate the time τ_{col} as $2R_{max}\sqrt{\frac{\mu}{2E}}$, where R_{max} represents the maximum distance of integration of the coupled equations. The distance R_{max} depends on the collision energy and is chosen so that the integration of our coupled equations leads to a convergent collisional **S** matrix and cross sections, σ. For example, R_{max} is taken as 100 a_0 at 0.1 meV, 40 a_0 at 10 meV, and 25 a_0 for $E \geq 30$ meV. The effective time of collision decreases from 139 ps at $E=0.1$ meV, to 0.35 ps at 1 eV and 0.2 ps at 3 eV. The time τ_{so} varies from 2.75×10^{-15} s (the shortest) for the $[2p_2(1), 2p_1(0)]$ states to 89.4×10^{-15} s (the longest) for the $[2p_3(0), 2p_4(2)]$ states. Because $\tau_{so} \ll \tau_{col}$, the orbital and spin momenta couple during the collision and form a net electronic angular momentum $\vec{J}$, which should be explicitly included in our quantum model.

III. COMPARISON BETWEEN THEORY AND EXPERIMENTS

Figure 1 shows a comparison between our close-coupling many-channel quantum calculations using the potentials proposed by Bahrim *et al.* [11] and the disalignment rate coefficients (K^{DA}) for the $Ne^*(2p_2)$, $Ne^*(2p_5)$, and $Ne^*(2p_7)$ atoms induced by isotropic collisions with He atoms measured with a polarization resolved LIFS method [4–6]. Our present calculations for K^{DA} of the $Ne^*(2p_2)$ atoms are performed over a wider temperature range, $T \leq 3000$ K, than in [12] where $T \leq 1000$ K. Therefore, now a wider collision energy range, $E \leq 3$ eV, is required for the integration of Eq. (2)

than it was necessary in Ref. [12], where $E \leq 1$ eV. Our test of convergence for K^{DA} using potentials from Ref. [11] shows that at $T=3000$ K the integration of Eq. (2) done up to 3 eV is 0.5% [for $Ne^*(2p_2)$], 0.6% [for $Ne^*(2p_5)$], and 0.3% [for $Ne^*(2p_7)$] larger than the integration done up to 2.4 eV. Therefore, excellent convergence for K^{DA} is obtained in all cases.

In Ref. [12] we show that using a repulsive long-range potential instead of the original potential from [11] shifts the intramultiplet cross section σ_{10} between the magnetic sublevels $M=1$ and 0 of the $2p_2$ level, and implicitly the variation in K^{DA} with temperature, upward, while an attractive long-range potential shifts σ_{10}, and implicitly K^{DA}, downward. The agreement with the experimental data from Refs. [5,6] for K^{DA} of the $Ne^*(2p_2)$ atoms is reached when our long-range potential is slightly more repulsive [12].

In Fig. 1 we show our results for K^{DA} of the $Ne^*(2p_2)$, $Ne^*(2p_5)$, and $Ne^*(2p_7)$ atoms using potentials from Ref. [12]. The long-range potential modifies K^{DA} stronger in the low temperature range than at large temperatures, because the long-range interaction affects mostly the cross sections for slow collisions [11]. As one can see in Fig. 1, our quantum calculation for the $Ne^*(2p_2)$ atoms is in agreement with the experimental data from Refs. [4–6], while a strong disagreement is observed for the $Ne^*(2p_5)$ and $Ne^*(2p_7)$ atoms. This situation suggests that no unique potential can correctly describe the disalignment of *all* the $Ne^*(2p_i[J=1])$ atoms induced by collisions with He atoms, as we initially assumed in our previous quantum calculations [5,10].

Figure 2 shows a comparison between our calculations for the energy-averaged cross sections of the alignment destruction ($\sigma^{(2)}$) for the $Ne^*(2p_2)$, $Ne^*(2p_5)$, and $Ne^*(2p_7)$ atoms induced by isotropic collisions with He atoms and the measurements from Ref. [8]. Our calculations use the potentials from Refs. [11,12]. The experimental data are extracted from the analysis of the Hanle signals [7] emitted by Ne^* atoms at thermal equilibrium with the He atoms in a gaseous mixture at 85 and 315 K [8].

The alignment destruction includes not only the atomic relaxation due to intramultiplet transitions, as in the case of the atomic disalignment, but also the excitation transfer toward other fine-structure states due to intermultiplet transitions as proved in [3,10]. Figure 2 shows that the intermultiplet transitions have a larger contribution to $\sigma^{(2)}$ as the temperature increases and have a negligible contribution below 77 K. The experimental data for $\sigma^{(2)}$ of the $Ne^*(2p_2)$ atoms are slightly larger than our calculations based on the potential from Ref. [11] when the temperature is lower, while for the $Ne^*(2p_7)$ atoms there is excellent agreement between theory and experiment at 85 and 315 K [8]. The same situation was observed for K^{DA} in Fig. 1. For the $Ne^*(2p_5)$ atoms, our results for $\sigma^{(2)}$ are much larger than those from Ref. [8] at 85 and 315 K.

Our present calculations for $\sigma^{(2)}$ of $Ne^*(2p_2)$ and $Ne^*(2p_7)$ atoms are performed over a wider temperature range than in [10], where $T \leq 650$ K. Our test of convergence for $\sigma^{(2)}$ of the $Ne^*(2p_2)$, $Ne^*(2p_5)$, and $Ne^*(2p_7)$ atoms calculated with Eq. (1) and using potentials from [11] shows that at 3000 K, the integration of Eqs. (2) and (3) done up to $E=3$ eV is about 0.3% larger than the integration done up to 2.4 eV only, when the de-excitations are included, and is 0.5% larger when the de-excitations are eliminated.

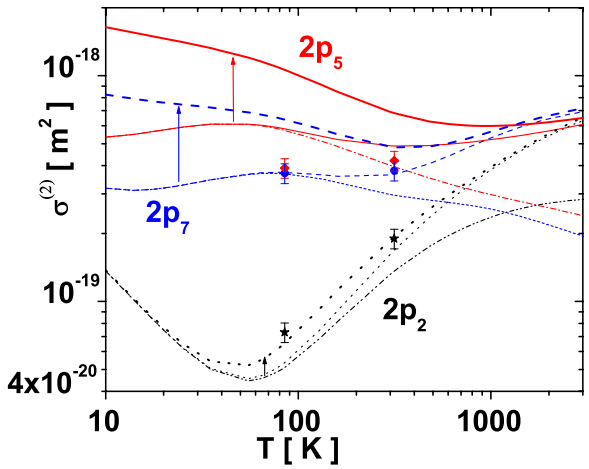

FIG. 2. (Color online) Energy-averaged cross sections for the alignment destruction ($\sigma^{(2)}$) of the $Ne^*(2p_2)$, $Ne^*(2p_5)$, and $Ne^*(2p_7)$ atoms: comparison between our quantum calculations (lines) using potentials from Refs. [11,12] and measurements from Ref. [8] (symbols) for the $2p_2$ (stars), $2p_5$ (diamonds), and $2p_7$ (dots) states. The experimental error bar is explicitly indicated. Our calculations including the intra- and intermultiplet transitions and using the potentials from Ref. [11] are shown by thin lines, while those using the potentials from Ref. [12] are shown by thick lines. The line style used for each $2p_i$ state is as in Fig. 1. The arrows indicate the shift upward of $\sigma^{(2)}$ when the potentials from Ref. [12] are used instead of those from Ref. [11]. For comparison, we also show calculations done including intramultiplet transitions only, and using potentials from Ref. [11] for $2p_2$ (dash-dot-dot line), $2p_7$ (short-dash line), and $2p_5$ (dash-dot line).

We observe big differences between the variations in K^{DA} and $\sigma^{(2)}$ for the $Ne^*(2p_2)$ and $Ne^*(2p_7)$ atoms calculated with potentials from [11,12]. In particular, our calculations for K^{DA} (Fig. 1) and $\sigma^{(2)}$ (Fig. 2) of the $Ne^*(2p_7)$ atoms using potentials from Ref. [11] agree well with data from Refs. [4,5,8] respectively, for 77 $K \leq T \leq 650$ K. However, below 35 K our K^{DA} decreases slower than the measurements from [5] because of a stronger rotational coupling between collisional channels at large internuclear distance, as discussed in Ref. [12].

When the potentials from Ref. [12] are used in our quantum calculations for $\sigma^{(2)}$ of $Ne^*(2p_2)$ atoms, excellent agreement with experimental data from [8] is found, while for the $2p_5$ and $2p_7$ states, our $\sigma^{(2)}$ cross sections are much larger than the data from [8]. This situation supports our previous hypothesis that no unique potential could describe the atomic interactions which are responsible for the alignment relaxation of *all* the $Ne^*(2p_i[J=1])$ atoms induced by Ne^*-He collisions.

Figure 3 shows that the long-range part of all collisional channels ($2p_i[J=1]$) is similar. All the channels are repulsive for $R > 8.5$ a_0 because they are dominated by the same spherically symmetric repulsive potential, V_σ, associated to the $e^-(3p)-$He interaction [10–12]. Figure 3 shows that a shift upward of the $2p_7$ collisional channel toward the $2p_5$ channel by an energy equal with the asymptotic energy dif-

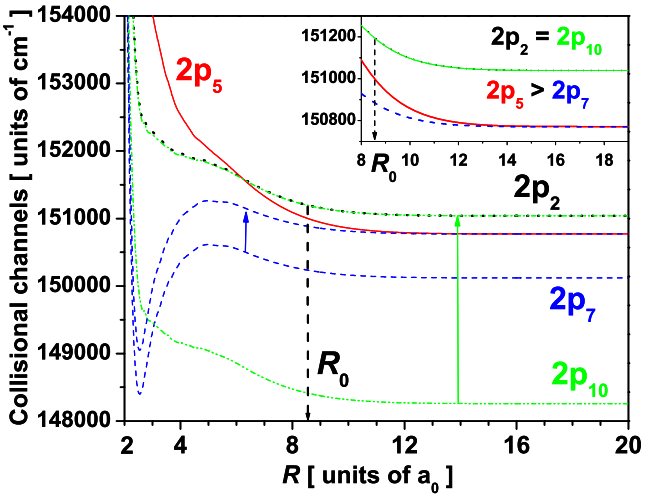

FIG. 3. (Color online) Selected collisional channels for the $\Omega=0^-$ symmetry which asymptotically converge toward the $Ne^*(2p_i[J=1])$ atomic states: the $2p_{10}$ (dash-dot-dot line) and $2p_7$ (dashed line) collisional channels are shifted upward by the energy difference between the $2p_{10}$ and $2p_2$ (dotted line) atomic levels, and the $2p_7$ and $2p_5$ (solid line) atomic levels, respectively. This shift helps us to make a comparison between the pairs of channels $(2p_{10},2p_2)$ and $(2p_7,2p_5)$, and to see their resemblance at large distances. In the inset we show for more clarity the same two pairs of channels superimposed at large R. At distances larger than R_0 of 8.5 a_0, the overall Ne^*-He interaction is dominated by the $V_\sigma(R)$ potential of the $e^-(3p)-$He interaction, according to Ref. [11].

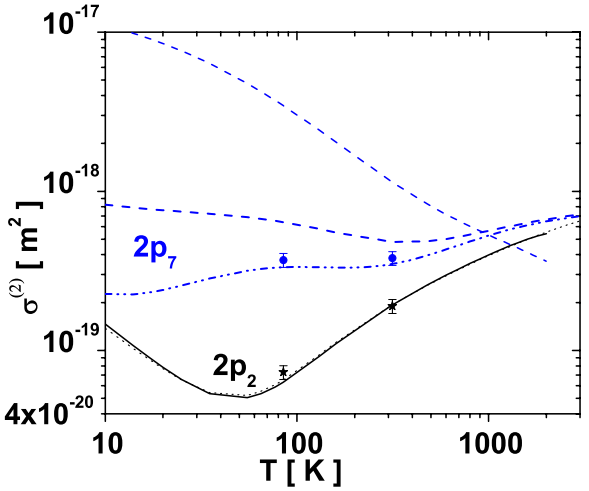

FIG. 4. (Color online) Study of $\sigma^{(2)}$ for the $Ne^*(2p_2)$ and $Ne^*(2p_7)$ atoms: comparison between experiments (symbols) from [8] and our calculations (lines) for (i) $2p_2$ using the potentials from Ref. [12] (dotted line) and by adding a dipole polarizability α_{2p_2} of +4.922 a.u. (solid line) to the potentials from Ref. [11], and (ii) $2p_7$ using the potentials from Ref. [12] (thick dashed line), and potentials which include at large R a dipole polarizability α_{2p_7} of +81.505 a.u. (thin dashed line) taken from [8] or −1.384 a.u. (dash-dot-dot line). The experimental error bar is explicitly indicated. Our calculations include both intra- and intermultiplet transitions.

ference between the $Ne^*(2p_5)$ and $Ne^*(2p_7)$ atomic levels makes the $2p_7$ and $2p_5$ channels to overlap for $R>14$ a_0. This overlap may explain the similar upward shift of K^{DA} (Fig. 1) and $\sigma^{(2)}$ (Fig. 2) for the $Ne^*(2p_5)$ and $Ne^*(2p_7)$ atoms at low T. Despite the repulsive character of all the $(2p_i[J=1])$ channels at large R (Fig. 3), the inclusion of a more repulsive potential [12] allows to attain agreement between theory and experiment for $Ne^*(2p_2)$, but worsens it for $Ne^*(2p_5)$ and $Ne^*(2p_7)$. Next, we will improve the model potential from [11] by introducing an additional long-range potential term, which will be state dependent.

IV. REVISION TO THE LONG-RANGE INTERACTION BETWEEN $Ne^*(2p_2[J=1])$ AND He ATOMS

When the wave function associated to a quantum particle does not penetrate significantly a neighbor atom then the electrostatic interaction can be typically described using a multipole expansion [16]. In this case, the description of the long-range interaction between atoms is done with a dipole polarization potential $(\sim\frac{1}{R^4})$ Our analysis of the He $Ne^+(2p^5)$ molecular ion from Ref. [11] led to the conclusion that the core-core interaction is precisely described by a dipole polarization potential $-\frac{\alpha_d}{2R^4}$ for $R>5.6$ a_0, where α_d is the dipole polarizability of the He ground-state atom (which is 1.384 a.u. from [17]). As opposed to a more compact $Ne^+(2p^5)$ ion, the $2p_i$ electron of Ne^* has a larger delocalization. Therefore, the dipole interaction between a polarizable $Ne^*(2p_i)$ atom and $He(1s^2)$ atom should occur at distances much larger than 5.6 a_0.

In Table IV of Ref. [8], Carrington and Corney have calculated static dipole polarizabilities for various $Ne^*(2p_i)$ atoms $(i=2,\ldots,10)$ assuming a simple theoretical model in which the interatomic force acting between the $Ne^*(2p_i)$ atom and the He perturber is due to the electrostatic dipole-dipole interaction, only. The atomic polarizabilities reported in [8] indicate that $Ne^*(2p_i)$ interacts differently with He for different $2p_i$ states: if the atomic polarizability is positive, then the overall $Ne^*(2p_i)-$He interaction is more repulsive, while for a negative atomic polarizability this interaction is more attractive. Quantum calculations for the $Ne^*(2p_2)$ state including the absolute value of the dipole polarizability (+4.922 a.u.) from [8] lead to excellent agreement with the available experimental data for the alignment relaxation (Fig. 4).

Next, we will briefly explain the way we incorporate the dipole polarizability potential in our present calculations, taking as example the $Ne^*(2p_2)$ case, and compare these calculations with those from Ref. [12], as well as with measurements from Refs. [4–6,8].

In Ref. [12], the long-range electrostatic potential is an adjustable dipole polarization term added to the $e^-(3p)-$He interaction described by the potential $V_\sigma(R)$ from Ref. [11]:

$$\tilde{V}_\sigma(R) = V_\sigma(R) + c * W_\sigma(R). \quad (4)$$

The core-core potential $W_\sigma(R)$ is given by $-\frac{\alpha_d}{2R^4}$ for $R>5.6$ a_0, according to [11]. The second term in Eq. (4) includes the R-dependent parameter c given by a Boltzmann sigmoidal function

$$c = \frac{3.7}{1 + \exp\left(\frac{R[\text{units of } a_0] - 13}{0.8}\right)} - 6.2. \quad (5)$$

If we set

$$\frac{\alpha_{2p_2}}{2R_c^4} = c(R_c) * W_\sigma(R_c), \quad (6)$$

where $\frac{\alpha_{2p_2}}{2R^4}$ is the dipole polarization potential between a polarizable $Ne^*(2p_2)$ atom and the He ground-state atom, then we can find a distance R_c for which the following equality holds:

$$\alpha_{2p_2} = -c(R_c) * \alpha_d. \quad (7)$$

Equation (7) allows us to calculate the value of the coefficient c for a given atomic polarizability α_{2p_2}. We choose α_{2p_2} as +4.922 a.u., which represents the absolute value of the polarizability given in Ref. [8]. This choice is consistent with our conclusion from Ref. [12] regarding a more repulsive character of the long-range potentials for the $Ne^*(2p_2)$-He interaction than it was reported in Ref. [11]. Using a polarizability α_{2p_2} of +4.922 a.u. in Eq. (7) leads to a coefficient c of −3.556. Further, using this value of c in Eq. (5) we find that R_c is 12.266 a_0, which is a value located between 9.75 a_0 and 13.5 a_0, in agreement with Ref. [12]. This result indicates that the calculations done with a polarization potential $\frac{\alpha_{2p_2}}{2R^4}$ are equivalent with those from Ref. [12].

Our present quantum calculations for the $Ne^*(2p_2)$+He collisions use potentials from Ref. [12] up to 12.266 a_0, from where a dipole polarization $\frac{\alpha_{2p_2}}{2R^4}$ term (with α_{2p_2} of +4.922 a.u.) is added to the long-range potentials from Ref. [11]. For $R \geq 12.266$ a_0, our new potentials are less than 28% different with respect to those from Ref. [12], the largest shift, of 28%, being at 13.5 a_0. The new potentials change our quantum results for atomic alignment relaxation by less than 5%, which is less than the experimental error bar from Refs. [4–6,8], of at least 10%. Figure 4 shows excellent agreement between calculations for the alignment destruction of $Ne^*(2p_2)$ atoms using the new polarization potential and measurements from Ref. [8]. This agreement validates our conclusion from Ref. [12] regarding the strong influence from the long-range part of the atom-atom potentials on the $Ne^*(2p_2)$+He collisions.

Next, we will improve our long-range potentials from Ref. [11] with the inclusion of the dipole polarizabilities for other $(2p_i[J=1])$ states and compare our results with the available measurements. We generalize Eqs. (4) and (6) to other $Ne^*(2p_i[J=1])$+He collisions as follows:

$$\tilde{V}_\sigma(R \geq R_c) = V_\sigma(R) + \frac{\alpha_{2p_i}}{2R^4}. \quad (8)$$

Our dipole polarizabilities α_{2p_i} for $Ne^*(2p_i[J=1])$ atoms will be compared with data from [8].

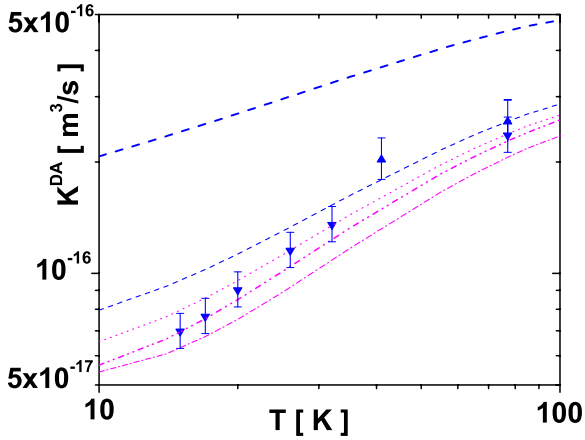

FIG. 5. (Color online) Study of K^{DA} for the $Ne^*(2p_7)$ atoms at low T: comparison between experimental data from [4] (triangle up), [5] (triangle down) and our calculations using (i) the potentials from Ref. [11] (thin dashed line), (ii) our more repulsive long-range potentials from Ref. [12] (thick dashed line), and (iii) the potentials based on Eq. (8) with R_c of 14 a_0 (dotted line), 15 a_0 (dash-dot-dot line), and 15.5 a_0 (dash-dot line).

V. DIPOLE POLARIZABILITIES FOR THE $Ne^*(2p_5)$ AND $Ne^*(2p_7)$ ATOMS

As shown in Figs. 1 and 2, our calculations using the potentials from Ref. [11] for the alignment relaxation of the $Ne^*(2p_7)$ atoms at $T > 77$ K are in good agreement with the experiments from Refs. [4,5,8]. However, for $T < 77$ K our calculations for K^{DA} are slightly larger than the data from [5], as shown in Fig. 1. Quantum calculations for $\sigma^{(2)}$ using α_{2p_7} of +81.505 a.u. (from Ref. [8]) in Eq. (8) give a strong disagreement with the experimental results given in [8] at any T. As example, in Fig. 4 we show the $\sigma^{(2)}$ cross section for the $Ne^*(2p_7)$ atoms.

A careful analysis led us to the conclusion that the polarizability of the $Ne^*(2p_7)$ state should be actually negative and smaller in absolute value than for the $Ne^*(2p_2)$ state. Our search led to the conclusion that excellent agreement with the experiments from [4,5,8] at any T is attained when α_{2p_7} of −1.384 a.u. is used in Eq. (8). Figure 5 shows results for K^{DA} of the $Ne^*(2p_7)$ atoms. The inclusion of a dipole polarization potential, $\frac{\alpha_{2p_7}}{2R^4}$, in Eq. (8) should be done at a distance R_c larger than for the $Ne^*(2p_2)$ atom (where $R_c = 12.266$ a_0), because a $2p_7$ electron has a lower energy than a $2p_2$ electron. Therefore, the average location of a $2p_7$ electron should be closer to the atomic $Ne^+(2p^5)$ core than of a $2p_2$ electron. We expect that closer is the charge distribution of a $2p_i$ electron to the atomic core, smaller the polarizability of the $Ne^*(2p_i)$ state and lesser is its influence to the overall long-range potential. In such a case, the $\frac{\alpha_{2p_i}}{2R^4}$ potential contributes to the overall long-range potential in Eq. (8), from larger distances R_c.

We tried several values for R_c and a few selected cases are shown in Fig. 5. We found that the best agreement with the experimental data for the $Ne^*(2p_7)$ state is reached at $R_c = 15$ a_0, which is indeed larger than for the $Ne^*(2p_2)$ state (of 12.266 a_0), and therefore, it supports the argument based

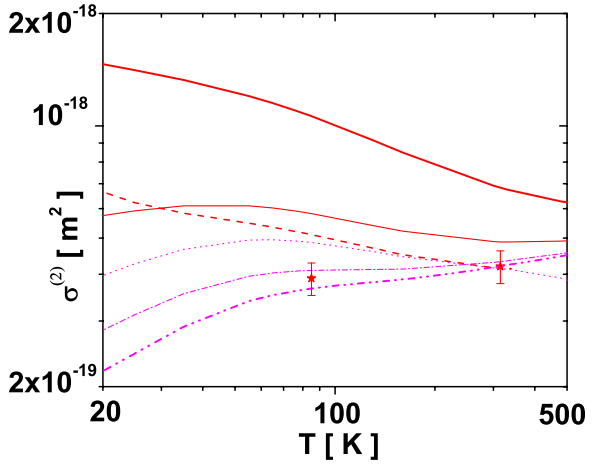

FIG. 6. (Color online) Study of $\sigma^{(2)}$ for the $Ne^*(2p_5)$ atoms: comparison between experiments (stars) from [8] and our calculations using (i) potentials from Ref. [11] (thin solid line), (ii) potentials from Ref. [12] (thick solid line), and (iii) using in Eq. (8) an additional α_{2p_5} of −28 a.u. (thick dashed line) and −2.768 a.u. with $R_c=15$ a_0 (dotted line), 14 a_0 (dash-dot line), and 13 a_0 (dash-dot-dot line).

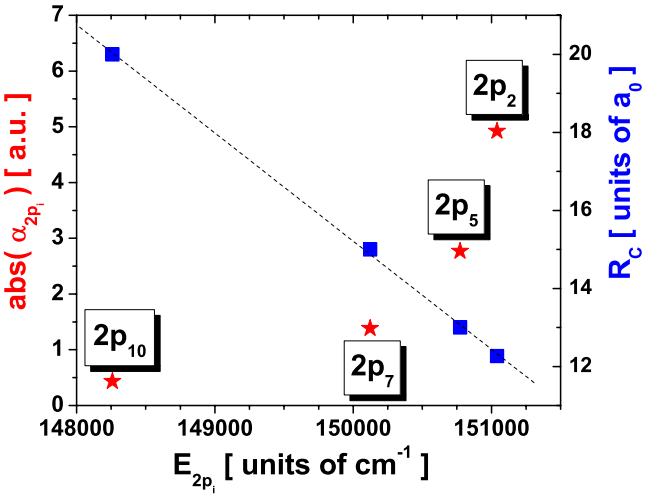

FIG. 7. (Color online) The variation in R_c (squares) and of the absolute value of the dipole polarizability, abs(α_{2p_i}) (stars), with the atomic energy, E_{2p_i}, of the $Ne^*(2p_i[J=1])$ states.

on the average location of the electronic charge distribution, discussed above.

We performed a similar study for the $Ne^*(2p_5)$ state. Because there are no experimental data for the disalignment of the $Ne^*(2p_5)$ atoms published yet, we calculate the polarizability of the $2p_5$ state using only the experimental data for the destruction of alignment reported in Ref. [8]. As for the $Ne^*(2p_7)$ case discussed in Fig. 4, using the dipole polarizability of the $Ne^*(2p_5)$ state from Ref. [8] (of −140.86 a.u.) leads to $\sigma^{(2)}$ values strongly shifted upward. Figure 6 shows our calculations with a smaller dipole polarizability, of −28 a.u. (which is about five times smaller than the value of −140.86 a.u. proposed in [8]), in order to make possible a graphic comparison with other theoretical trials. The best agreement with the experimental data from [8] is found when a much smaller polarizability α_{2p_5}, of −2.768 a.u., is used in our calculations.

The search for the best agreement between theory and experiment led us to $R_c=13$ a_0, which is located between 12.266 a_0 (for $2p_2$) and 15 a_0 (for $2p_7$), as expected for a $2p_5$ level located between $2p_2$ and $2p_7$. A couple of other relevant cases for our choice of R_c are shown in Fig. 6. The test of convergence for the collision energy range ($E \leq 3$ eV) employed in our present calculations for the $Ne^*(2p_2)$, $Ne^*(2p_5)$, and $Ne^*(2p_7)$ atoms using the new long-range potential from Eq. (8) and our best dipole polarizabilities according to Figs. 4–6 leads to variations smaller than 0.5% for both K^{DA} and $\sigma^{(2)}$, when calculations done up to 2.4 and 3 eV are compared.

In conclusion, we observe that the contribution of the $\frac{\alpha_{2p_i}}{2R^4}$ term in Eq. (8), to the long-range electrostatic potential between helium and $Ne^*(2p_2)$, $Ne^*(2p_5)$, or $Ne^*(2p_7)$ atoms, depends on the average position of the electronic charge distribution of each $2p_i$ state in the vicinity of the $Ne^+(2p^5)$ core. We see that for a $Ne^*(2p_i)$ atom larger in size (and with a larger energy), the magnitude of the dipole polarizability is bigger and the distance R_c from where the polarization potential $\frac{\alpha_{2p_i}}{2R^4}$ has to be included in Eq. (8) is smaller. This is expected to be so, because a large atomic polarizability has to have a stronger influence on the alignment relaxation of atoms during collisions at shorter internuclear distances. Figure 7 shows that the absolute value of the dipole polarizability α_{2p_i}(with $i=2,5,7$) increases quasi-exponentially with the increase in the energy level of the $Ne^*(2p_i[J=1])$ atoms, while R_c varies linearly with this energy.

VI. ALIGNMENT RELAXATION OF THE $Ne^*(2p_{10})$ ATOMS INDUCED BY Ne^*–He COLLISIONS

Due to a lack of experimental data for the alignment relaxation of the $Ne^*(2p_{10})$ atoms induced by collisions with He ground-state atoms, in our quantum calculations we adopt the same value of 0.432 a.u. for the polarizability of the $Ne^*(2p_{10})$ state as reported in [8]. However, we take a positive rather than negative value for $\alpha_{2p_{10}}$, as given in Table IV of Ref. [8], because we observe a strong resemblance between the $2p_{10}$ and $2p_2$ collisional channels. As shown in Fig. 3, a shift upward of the $2p_{10}$ collisional channel by the energy difference between the asymptotic $2p_{10}$ and $2p_2$ atomic levels leads to an almost perfect overlap between the two channels for distances $R>4$ a_0. For $R>8.5$ a_0, both $2p_{10}$ and $2p_2$ channels are repulsive.

A linear extrapolation toward the $Ne^*(2p_{10})$ state from the dependence of R_c with the atomic energies of the $Ne^*(2p_i)$ states from Fig. 7 suggests that R_c should be 20 a_0 for the $Ne^*(2p_{10})$ atom. Our quantum calculations for alignment relaxation of the $Ne^*(2p_{10})$ atoms using $\alpha_{2p_{10}}$ of +0.432 a.u. and $R_c=20$ a_0 are given in Figs. 8 and 9.

Our study for the $Ne^*(2p_{10})$+He collision indicates that the alignment relaxation of the $Ne^*(2p_{10})$ atoms is much less sensitive to the choice of the long-range potential as compared with the other three states with $J=1$ of the $2p^5 3p$ con-

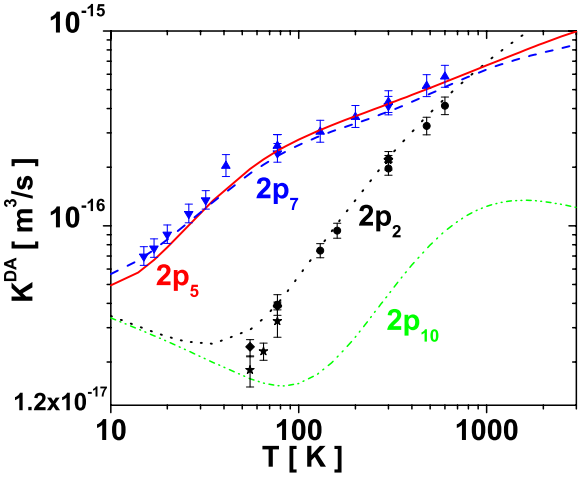

FIG. 8. (Color online) Comparison between measurements (symbols) from Refs. [4–6] and our calculations (lines) for K^{DA} using the long-range potentials based on Eq. (8) and the atomic dipole polarizabilities: $\alpha_{2p_2}=+4.922$ a.u. ($R_c=12.266\ a_0$), $\alpha_{2p_5}=-2.768$ a.u. ($R_c=13\ a_0$), $\alpha_{2p_7}=-1.384$ a.u. ($R_c=15\ a_0$), and $\alpha_{2p_{10}}=+0.432$ a.u. ($R_c=20\ a_0$). The symbols and the lines style are similar as in Fig. 1. For K^{DA} of the Ne*($2p_{10}$) atoms our calculations are shown by a dash-dot-dot line. The experimental error bar is given explicitly.

figuration of neon. Calculations done with (i) the repulsive potential from Ref. [12], (ii) an additional polarizability of 0.432 a.u. or (iii) using our initial potentials from Ref. [11] are all different by less than 1%. This situation makes that all our theoretical curves for the alignment relaxation of the Ne*($2p_{10}$) atoms induced by collisions with He atoms to overlap in Fig. 8 (for disalignment) and Fig. 9 (for destruction of alignment). Of course, both values for the polarizability $\alpha_{2p_{10}}$ and the distance R_c for the $2p_{10}$ case can be reanalyzed when experimental data will be available. However,

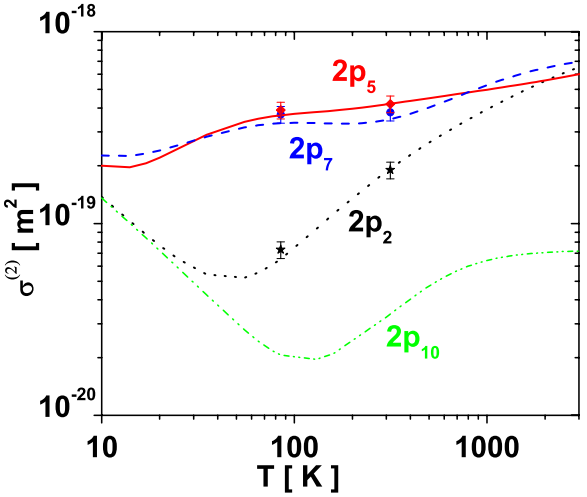

FIG. 9. (Color online) Comparison between measurements (symbols) of $\sigma^{(2)}$ from Ref. [8] and our calculations using the long-range potentials from Eq. (8) for the same values of α_{2p_i} and R_c as in Fig. 8. The symbols and the line style used for each $2p_i$ state are as in Fig. 8. The experimental error bar is explicitly indicated.

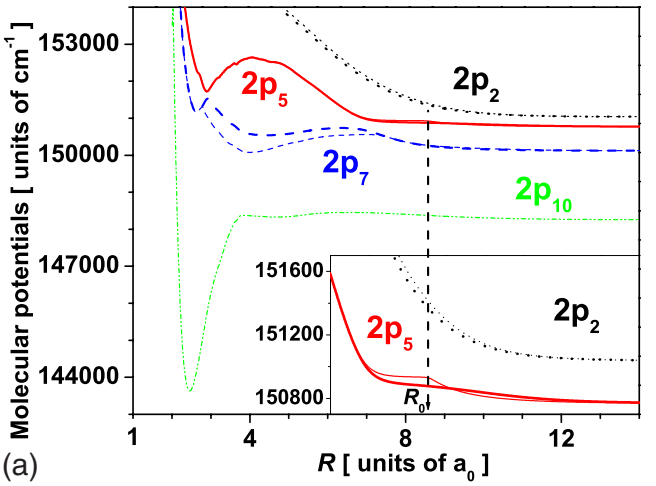

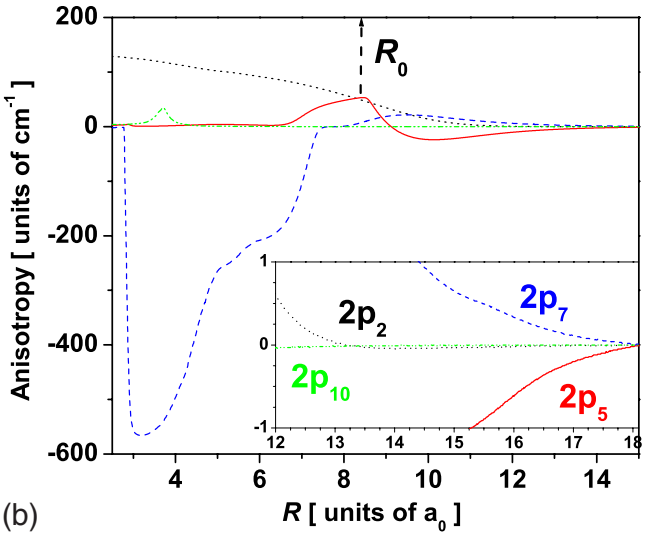

FIG. 10. (Color online) (a) Selected molecular states of the HeNe*($2p_i[J=1]$) system, with $\Omega^{\pi}=1$ (thin lines) and 0^- (thick lines), converging asymptotically toward the $J=1$ atomic states: Ne*($2p_2$) (dotted lines), Ne*($2p_5$) (solid lines), Ne*($2p_7$) (dashed lines), and Ne*($2p_{10}$)(dashed-dotted-dotted lines); (b) the anisotropy between the $\Omega^{\pi}=1$ and 0^- molecular states of the HeNe($2p^5 3p$) system for the same $J=1$ atomic states, which are shown in (a). The line style in (b) is the same as in (a) for the same states. The distance R_0 is 8.5 a_0, and it was defined in Fig. 3.

we consider that it is important to report this first calculation for the alignment relaxation of the Ne*($2p_{10}$) atoms here, because of the interest in having theoretical data available for guiding new experiments, such as the LIFS experiments currently underway at Kyoto University in the group of Professor Hasuo [18].

Calculations of alignment relaxation for all the $J=1$ states of the $2p^5 3p$ configuration of neon [Ne*($2p_2$), Ne*($2p_5$), Ne*($2p_7$), and Ne*($2p_{10}$) atoms] induced by collisions with He atoms are reported in Fig. 8 (for K^{DA}) and Fig. 9 (for $\sigma^{(2)}$). Very good agreement with the available experimental data is found everywhere except for the $2p_2$ case at temperatures below 77 K. This problem was addressed in Ref. [12] and an explanation based on the influence of the Coriolis (rotational) coupling between the $\Omega=0^-$ and $\Omega=1$ collisional

channels was proposed. The strong resemblance between the $2p_2$ and $2p_{10}$ collisional channels shown in Fig. 3 suggests that a similar influence from the Coriolis coupling should exist for large internuclear distances in the $Ne^*(2p_{10})+He$ collision, too. This coupling could explain the increase in our theoretical K^{DA} for the $Ne^*(2p_{10})$ atoms, as well as the convergence of K^{DA} toward the same limit as for the $Ne^*(2p_2)$ atoms, below 20 K. This result indicates that the atomic disalignment at very low temperatures strongly depends on the dynamic interaction due to the rotational coupling between collisional channels at very large internuclear distances [12].

The atomic alignment relaxation offers information about the anisotropic interaction between atoms. We define the anisotropy of the $Ne^*(2p_i[J=1])+He$ collision as the difference between the energy of the adiabatic potentials in various Ω^π symmetries. For the $J=1$ states of the $2p^5 3p$ configuration of neon, the anisotropy is the energy difference between the molecular states with $\Omega^\pi=1$ and 0^-. The molecular states of the $HeNe^*(2p_i[J=1])$ system are shown in Fig. 10(a) and their anisotropy is given in Fig. 10(b). For the $Ne^*(2p_{10})$ case, the anisotropy between the two adiabatic states is very small for any R. This explains the lack of sensitivity of our calculations for the alignment relaxation of the $Ne^*(2p_{10})$ atoms with the change in the long-range potentials. Also, the anisotropy of other molecular states can explain the difference in the magnitude of the alignment relaxation rates of the $Ne^*(2p_i[J=1])$ atoms reported in Figs. 8 and 9. Thus, for the $Ne^*(2p_5)$ and $Ne^*(2p_7)$ molecular states, the anisotropy is larger at large R [as shown in the inset of Fig. 10(b)] than for $Ne^*(2p_2)$, while for $Ne^*(2p_{10})$, the anisotropy is the smallest. This situation makes the alignment relaxation of $Ne^*(2p_5)$ and $Ne^*(2p_7)$ atoms much larger at lower temperatures than of the $Ne^*(2p_2)$ and $Ne^*(2p_{10})$ atoms. The almost identical (small) anisotropy of the molecular states associated to the $Ne^*(2p_{10})$ and $Ne^*(2p_2)$ atoms at large R makes our theoretical K^{DA} and $\sigma^{(2)}$ to have a similar variation at low temperatures, as shown in Figs. 8 and 9.

VII. CONCLUSION

Comparison between our quantum calculations using the potentials from [11,12] and experiments for alignment relaxation (disalignment [4–6] and alignment destruction [8]) due to collisions between the $Ne^*(2p_2)$, $Ne^*(2p_5)$, and $Ne^*(2p_7)$ atoms and the $He(1s^2)$ atoms in a gaseous mixture at thermal equilibrium suggests that the long-range $Ne^*(2p_i[J=1])-He$ potentials should include an additional polarization potential, $\frac{\alpha_{2p_i}}{2R^4}$, for each of the $2p_i[J=1]$ states. Excellent agreement between our calculations and various experiments is then found for a wide temperature range. We have proposed the following set of dipole polarizabilities for the $Ne^*(2p_i[J=1])$ atoms: $\alpha_{2p_2}=+4.922$ a.u., $\alpha_{2p_5}=-2.768$ a.u., $\alpha_{2p_7}=-1.384$ a.u., and $\alpha_{2p_{10}}=+0.432$ a.u., and compare our values with those reported in Ref. [8]. Also, we identify an internuclear distance, R_c, from where the $\frac{\alpha_{2p_i}}{2R^4}$ potentials should be added to the long-range potentials from [11], and we observe a linear variation in R_c with the energy of the four $2p_i[J=1]$ atomic states of neon. In addition, we saw that the absolute value of the atomic dipole polarizability α_{2p_i} has an exponential increase with the atomic energies of the $2p_i[J=1]$ states and shows that a larger $Ne^*(2p_i[J=1])$ atom has larger dipole polarizability. Therefore, for large atoms the contribution of the $\frac{\alpha_{2p_i}}{2R^4}$ potential to the long-range electrostatic potentials starts from a smaller internuclear distance R_c than for smaller atoms. The values of the dipole polarizabilities for the $Ne^*(2p_5)$ and $Ne^*(2p_{10})$ atoms reported here could be further improved when more experimental data will be available.

ACKNOWLEDGMENTS

This work was encouraged through the interest manifested by Professor Masahiro Hasuo and Hiraku Matsukuma. We are very grateful for their input, suggestions, and for sharing with us their most recent experimental investigations.

[1] K. Blum, *Density Matrix Theory and Applications*, 2nd ed. (Plenum, New York, 1996).
[2] A. Omont, Prog. Quantum Electron. **5**, 69 (1977).
[3] T. Fujimoto and S. Matsumoto, J. Phys. B **21**, L267 (1988).
[4] T. Wakabayashi, A. Yamamoto, T. Yaneda, T. Furutani, A. Hishikawa, and T. Fujimoto, J. Phys. B **31**, 341 (1998).
[5] M. Seo, T. Shimamura, T. Furatani, M. Hasuo, C. Bahrim, and T. Fujimoto, J. Phys. B **36**, 1885 (2003).
[6] M. Nimura, M. Hasuo, and T. Fujimoto, J. Phys. B **37**, 4647 (2004).
[7] C. G. Carrington and A. Corney, J. Phys. B **4**, 849 (1971).
[8] C. G. Carrington and A. Corney, J. Phys. B **4**, 869 (1971).
[9] T. Fujimoto, C. Goto, and K. Fukuda, J. Phys. Soc. Jpn. **53**, 574 (1984).
[10] C. Bahrim, H. Kucal, O. Dulieu, and F. Masnou-Seeuws, J. Phys. B **30**, L797 (1997).
[11] C. Bahrim, H. Kucal, and F. Masnou-Seeuws, Phys. Rev. A **56**, 1305 (1997).
[12] C. Bahrim and V. V. Khadilkar, J. Phys. B **41**, 035203 (2008).
[13] D. Hennecart and F. Masnou-Seeuws, J. Phys. B **18**, 657 (1985).
[14] *Plasma Polarization Spectroscopy*, edited by T. Fujimoto and A. Iwamae (Springer, New York, 2007).
[15] T. Fujimoto and S. A. Kazantsev, Plasma Phys. Contr. Fusion **39**, 1267 (1997).
[16] H. Margenau and N. R. Kestner, *Theory of Intermolecular Forces*, 1st ed. (Pergamon Press, Oxford, 1969).
[17] A. Dalgarno and A. E. Kingston, Proc. R. Soc. London, Ser. A **259**, 424 (1960).
[18] M. Hasuo and H. Matsukuma (private communication).